technical memorandum Daresbury Laboratory

DL/SCI/TM56E

RAYTRACING WITH MAXRAY AND THE DESIGN OF PX STATION 9.5

by

R.C. BRAMMER, SERC Daresbury Laboratory and University of Uppsala

NOVEMBER, 1987

G87/633

Science and Engineering Research Council

DARESBURY LABORATORY

Daresbury, Warrington WA4 4AD

ISSN 0144-5677

Raytracing with MAXRAY and the design of PX station 9.5

R.C. Brammer

November 24, 1987

SERC Daresbury Laboratory, Warrington England

and

Dept. of Mol. Biol., Uppsala University, Uppsala Sweden

Abstract

This paper describes the use of the MAXRAY raytracing subroutines in designing beam line optics for station 9.5 at the Daresbury Laboratory. Examples of the effects of adjusting parameters on a toroidal mirror are shown and explained. A brief explanation of the use of the raytracing routines is given to facilitate use of the routines by others. Copies of the program code are available on request.

1 Introduction

The principle behind raytracing is to model the passage of a light ray through a system of optical elements using mathematical relationships. The light ray is simulated by a vector and optical operations such as reflection and diffraction are simulated by vector operations. By tracing the paths of many rays through the system one can create a picture of its expected optical properties. The reasons for doing this are clear, one can test different designs on the computer without having to actually construct them. Design points can be tested and particular sensitivites of the system can be detected at a stage early enough to provide design compensations. Once the optical elements have been chosen, guidelines for adjustment and use of the system can be provided. For example, a gazetteer of possible spot configurations can be generated to assist in focussing the system in its commissioning stages.

The primary purpose of this raytracing project was to test the properties of the focussing mirror to be installed on wiggler station 9.5. This will be a Protein Crystallography (PX) station and it is being financed jointly by the Swedish Natural Sciences Research Council (NFR) and the SERC Daresbury Laboratory. Figure 1

shows the schematic set up of the beam line [1]. The placement of the mirror on the beam line was dictated by the physical space available. This placement, at 18.325 m from the wiggler, plus the conditions of minimum aberration on the focal spot and the choice of shortest wavelength to be transmitted determine the physical appearance of the mirror [1]. For a single mirror to focus both horizontally and vertically the optimum surface is ellipsoidal, but these mirrors are difficult to fabricate so we have chosen a bendable cylinder which approximates a toroid mirror. Setting the focal point at 32.0 m from the tangent point (the center of the experimental hutch) and the incidence angle on the mirror to 3.0 mrad (setting the short wavelength cutoff at 0.44 Å for a platinum coating) one arrives at the parameters of the mirror. The radius of curvature for horizontal focussing is 46.9 mm and is machined into the surface of the 75 cm long mirror during the manufacturing process. The vertical focussing is accomplished by bending the cylinder to the desired radius with a bending mechanism. The radius of curvature for this focussing is 5221 m. This description of the mirror surface has been used as the standard for the raytrace series and all the raytraces included in this paper use this set of parameters as a starting point.

2 The Raytracing Principle

For this raytrace project the MAXRAY collection of subroutines, developed in Uppsala, was used [2]. There are other routines available (e.g. [3-5]) but this collection was chosen because of its adaptability. A preliminary study of the optics of 9.5 has been performed [6] using the raytracing methods described in ref. 3. The authors of the MAXRAY package have collected a set of subroutines written in FORTRAN 77 which the programmer can use to design almost any specific optical system. Because the subroutines were not written to simulate a specific synchrotron source they can be used anywhere, and have proven to be very useful for line 9.5. In the system, each element of the optical system is represented by a subroutine. A ray's progression through the system is accomplished by allowing it to move from one element to the next and constantly adjusting the frame of reference by rotation and translation subroutines to that of the element being simulated. When the specific subroutine is called, the initial position and direction of the ray is sent to the called subroutine, after the optical operation has been performed, a new position and direction are returned, along with various diagnostic values.

3 MAXRAY Subroutines

The subroutine set of the MAXRAY package includes a simulated bending magnet source. Input to this source defines the bending radius, the horizontal angle and vertical distribution full width at half maximum (FWHM). The routine generates random rays in the given source area and the vertical intensity distribution is simulated by the vertical FWHM. The resulting ray pattern approximates the intensity

of the synchrotron source where more rays are produced in the regions of higher intensity. User specific sources, including patterned sources may be used if desired. For this program a pattern source was developed where a source area could be defined and filled with a matrix of source points. Each of these points could then be the source of rays distributed equally over a range of horizontal and vertical angles within the limits of the source divergences.

To allow the ray to be transported through the system there are subroutines for translation and rotation of the coordinate system origin as well as a normalization routine. The optical elements included in the subroutines suite are for reflective surfaces and for diffraction grating surfaces of various geometrical shapes. The mirror surfaces subroutines include planes, cylinders (along two different directions for convenience), elipsoids, eliptical cylinders, paraboloids, plane-parabolas, spheres and toroids. The grating surfaces (which have not been a part of this study, but are included for completeness) include planes, spheres and toroids. Crystal monochromators can be approximated by sets of reflective surfaces where crystal characteristics (e.g. the correspondance between energy and incidence angle) are set by the calling program. Before calling the given optical element routine the boundaries are set. If the ray intersects the surface outside of the boundaries this is noted and a diagnostic is returned from the subroutine.

Slits, apertures and target areas are formed by calling a nonreflecting plane subroutine. This routine simply detects the intersection point of the ray with the surface. As with the reflective elements the boundaries are defined prior to calling the subroutine and diagnostics returned by the routine inform as to whether the ray has intersected the surface within the allowed area. A target area can be defined in the same way. The program output then consists of the coordinates of points where a ray intersects the given target surface. The raytraces included here show the rays intersecting a plane, located at the crystal or collimator, which is perpendicular to the central ray following the origins of the optical elements.

The number of rays passing through the system (or falling outside of the boundaries) can be counted at any element and in particular the number of rays successfully reaching a given area (at the position of the crystal) have been counted. For this paper, rays falling within a square area corresponding to that of a 0.3 mm diameter collimator have been used to determine success percentages and to provide comparisons between different configurations.

4 Elements used in this simulation

For this project a selected subset of the available routines has been used. The pattern source has been used to shed light on the aberrations introduced by the mirror surface. The bending magnet source has been used to simulate the wiggler source. With the radius set at 1.3 m this is a reasonable approximation of the monopole wiggler source, especially since station 9.5 utilizes radiation from the center of the 'fan' produced by the wiggler. The half 'wiggles' on either side of

the main 'wiggle' are not expected to contribute significantly to the intensity 'seen' by station 9.5 [7]. The simulated bending magnet source could be used to create subroutines simulating other sources such as multipole wigglers, but this has not been done for this project.

The mirror surfaces used for this simulation include plane mirrors, cylinder mirrors and toroid mirrors. The system was built up using successively more complicated surface geometries. For the monochromator, simulations of both plane and cylindrically curved mirrors have been used (with the reflection angle, i.e. the Bragg angle, as an input parameter). The apertures used include adjustable horizontal/vertical slits before the monochromator and the mirror. Finally a planar target surface at the position of the crystal has been used.

The program as originally written produced output using graphics routines suitable for Tektronix compatible terminals. This type of graphic data was only savable via a screen dump which was particularly inefficient for a large number of points. A further addition to the program produced output files with the coordinates of points intersecting the target plane as well as significant parameters. This point data can be used by subsidiary graphics programs based on GHOST plot routines, providing convenient hardcopy possibilities. By dividing the target surface into an array of areas, surfaces with the vertical height corresponding to relative intensity can be produced. Again the data is routed to a file which can be used by subsidiary programs utilizing GHOST routines to plot 3-d surfaces or contours. Examples of all the types of output are include in the figures. The actual FORTRAN code of the program used is is too extensive to be included here but is available to anyone on request. It should be pointed out that it was never the intention to circulate the program as written for general use since it evolved freely over a period of time and has not been streamlined. Nevertheless it could provide insight into how the MAXRAY routines can be combined into a working unit. Readers are welcome to use any part of the program that they might find useful.

5 Results: Figure descriptions

5.1 Figures 2a, 2b, 3a and 3b

The raytracing results are illustrated by a series of plots where different parameter configurations have been examined. The plot shown in Figure 2a is the focal spot produced by the simulated synchrotron source when reflected from the toroidal mirror with parameters stated above, the ideal mirror for station 9.5. It should be pointed out that the focal spot has its greatest concentration of intensity (i.e. more plotted rays) in the area near the origin. In all of the raytraces the target origin is the point of maximum intensity from this ideal mirror and the scale is given in millimeters. Figure 2b shows the relation of the focal spot position to that of unreflected radiation. In this idealized study ALL rays missing the reflective surface are allowed to proceed to the target plane. One can clearly see the projection of

the reflective surface. This particular raytrace showed the feasibility of including a beryllium window approximately 8 cm below the focal spot to permit experiments with unfocussed light [1]. This unreflected light is not subject to the wavelength cutoff of the platinum coated mirror. Figures 3a and 3b are equivalent to 2a and 2b with a regular pattern source used. The source is taken to be a point source with divergences equal to those expected for 1 Å radiation. Note that Figure 3a has its origin at the center of the plot while Figure 2a has the origin shifted slightly upward (both plots in same scale).

5.2 Figures 4, 5a, 5b and 6

In order to see the effect of adjustment of the different mirror parameters it is instructive to begin with a plane mirror and to change only one parameter at a time. Figure 4 shows the effect of a plane reflective surface of the same physical dimensions as that of the toroid (75.0 cm by 4.0 cm reflecting surface). The reflected rays are centered at the origin as expected and apart from the displacement the reflected image is exactly like the projection of the mirror surface. Figures 5a and 5b show the effect of bending the plane mirror into a cylinder with a radius of 46.9 mm. The mirror focusses the radiation so that the horizontal extent of the focussed radiation is reduced to about 2 mm. The vertical size is not changed much although a certain amount of distortion can be seen in Figure 5b. Figure 6 shows the ideal focal spot (i.e. bending of the cylinder to a vertical radius of 5221 m) in the same scale as Figure 5b. Comparison between Figures 5b and 6 shows clearly the compression of the focal spot in the vertical direction when the vertical bend is applied.

5.3 Figures 7a, 7b, 8a and 8b

Figures 7a and 7b show what happens to the focal spot when the cylinder radius (i.e. horizontal radius) is set to the nonoptimal values of 46.5 and 47.5 mm respectively. The corresponding effects of the same horizontal radius adjustments on the toroid (with ideal vertical radius) are shown in Figures 8a and 8b.

5.4 Figures 9a and 9b

If one adjusts the vertical radius to values other than that of the optimum, the focal spot pattern begins to expand vertically again. Figure 9a shows the effect of decreasing the vertical radius to 3614 m (other parameters unchanged from the optimal for focussed spot). Figure 9b shows the corresponding pattern resulting from an increase of vertical radius to 8000 m.

5.5 Figures 10a and 10b

The angle of incidence upon the mirror is optimized at 3.0 mrad to allow a short wavelength cutoff by the platinum surface at 0.44 Å. If this angle is changed the effect on the focal spot is not simply a translation of the focal spot pattern as might be expected. Figures 10a and 10b show the effect of setting the graze angle to 2.9 and 3.1 mrad respectively. The smaller graze angle causes the focal spot pattern to enlongate as well as to be translated downward from the target origin. The larger graze angle results in a pattern which is ring shaped and above the target origin.

5.6 Figures 11a-11d, and 12a-12d

The experimental hutch has a length of 2.3 meters along which experiments can be centered. This region between 30.5 and 32.8 m from the tangent point of the wiggler bend can be used to position the different detection apparatus: traditional film cameras, the FAST area detector and image plates [1]. Although the permanent radius of the cylinder is optimized for 32.0 m focus, the vertical radius is adjustable as is the graze angle. By substituting the new focal distance into the equation of minimum aberration while holding the horizontal radius fixed at 46.9 mm, new optimizations of the vertical radius and incidence angle are obtained. Figures 11a to 11d show the steps to optimization at 32.8 m. Figure 11a shows the appearance of the focal spot at 32.8 m for the mirror with parameters optimized for 32.0 m. By comparing with Figure 6 one can see how the spot size expands as the target plane is moved further from the tangent point. Figure 11b shows the effect of adjusting to the appropriate graze angle. Figure 11c shows the effect of adjusting only the vertical radius. Finally, Figure 11d shows the spot obtained when both adjustments are made. The same procedure has been used to examine the spot appearances at 30.5 m. Figures 12a to 12d show the corresponding series of adjustments. Note that in Figures 12b and 12d the origin has been shifted to better show the focal spot.

5.7 Figures 13, 14, 15a and 15b

It is clear from Figure 2a that the full focal spot size from the entire reflective surface is larger than can be accepted by a typical collimator and improvements (with regards to amount of white radiation impinging on the mirror) can be made by limiting the acceptance of the mirror to 1.0 mrad horizontally and 0.1 mrad vertically. The effect of this limitation is shown in Figures 13 and 14 where Figure 13 shows a projection of how much of the mirror surface is actually used and Figure 14 shows the resulting focal spot. Spot counts show that 73 % of the radiation falling within the area of a collimator is retained after this masking of the mirror. The result of this masking of the mirror is similar at the longer and shorter focal distances described above. Figures 15a and 15b show the focal spots for 32.8 and 30.5 m respectively. Note that the centers of these plots have been shifted to better show the focal spots. Spot counts from these raytraces indicate that the mirror focussed

at 30.5 m receives 104.2 % of rays at 32.0 m (the increase due to greater acceptance at graze angle 3.21 mrad) and 93.7 % of the rays at 32.8 m.

5.8 Figures 16a, 16b, 17a and 17b

An alternative way of presenting the raytrace data is shown in the next figures. In these the raytrace program's surface output has been used. Figures 16a and 16b show from two separate angles the three dimensional surface derived from the masked spot of Figure 14. This same surface data is shown in contour form in Figure 17a and for a smaller area in 17b. It is quite easy to see the large concentration of radiation falling onto the area from the closeness of the contour lines. 50 % of the total intensity is contained in center area of 0.25 square mm; 20 % is contained in the area corresponding to a collimator of diameter 0.2 mm.

6 Results from incorrect mirror alignment

In all of the raytraces shown above the mirror was assumed to be perfectly aligned. The position of the toroid mirror can deviate from the correct in several ways and these have been tested. It can be rotated about an axis perpendicular to the mirror (yaw) or about an axis in the mirror plane perpendicular to the axis for adjusting incidence angle (roll). The mirror assembly has been designed to be retractable from the beam so the mirror can be incorrectly translated, resulting in positions either too high or too low.

6.1 Figures 18a, 18b, 18c and 19

The rotation of the mirror around an axis perpendicular to its surface, the yaw angle, was found to be extremely critical to the size of the focal spot. Figure 18a shows the extent of the focal spot when the mirror is rotated by only 0.2 mrad (compare with Figure 6). Figure 18b shows the same parameters using the pattern source described above. A small yaw adjustment rapidly changes the 'effective' radius seen by the synchrotron beam (that is the radius of the mirror formed by the intersection of a vertical plane through the synchroton beam and the surface of the mirror). Rotation by 1 mrad from the optimum causes the effective radius to change to 4698 m, causing the focal spot size to increase rapidly. Spot counts show that less than 1 % of the rays are retained after rotation of 1.0 mrad (15.5 % for 0.2 mrad yaw error). This observation has prompted us to include fine- stepper motors in the design which will permit adjustment of the yaw in fractions of a mrad [1]. Inclusion of the mirror mask which limits the acceptance to 1.0 mrad horizontally and 0.1 mrad vertically reduces the spot size from the rotated mirror to the one shown in Figure 18c. Related to the problem of yaw is the problem of movement of the source due to fluctuations in the electron orbits. Horizontal movement of the source by 1 mm along with an optimum mirror setting results in the focal spot shown in Figure 19.

6.2 Figures 20, 21a and 21b

The effect of a mirror roll of 20.0 mrad is shown in Figure 20. Translation of the mirror center to a position 1 mm below the optimum results in the focal spot seen in Figure 21a. Figure 21b shows the corresponding focal spot for the mirror positioned at 1 mm above the optimum. Figures 20 and 21 have been plotted at a different scale than the others so one should be aware of this when making comparisons.

7 Monochromator simulation

Some word should be said about the use of mirror surfaces to simulate monochromator crystals. Since the rays in the system have no specific energy, the principle value of including 'crystals' in the raytrace system is to determine the appropriate size to be used. One can easily easily see the effect in intensity of shortening the crystals since rays then fall outside the limits and are not allowed to proceed through the optical system. Small changes in the focal spot can be expected since the presence of the crystals changes slightly the distance the ray travels before striking the mirror. Finally one can expect the correlation between the horizontal and vertical divergences to be affected slightly. These effects are, however, very small and nothing significant was observed in the raytraces.

8 Conclusions

With this set of raytraces and others that have not been included here I have performed an analysis of the optical system to be installed on beam line 9.5. It has proved very helpful in testing the optical configuration and it has caused us to look carefully at things that might otherwise have been overlooked. I hope that this document will encourage others to use this method as well. I would like to recommend the raytrace package MAXRAY which I have used and found very easy to adapt to my specific problems.

Acknowledgements

I would like to acknowledge support in the form of a post doctoral fellowship from the Swedish Natural Sciences Research Council (NFR) and to Daresbury Laboratory for the facilities made available to work on this project.

References

[1] Daresbury Preprint DL/SCI/P567E (1987), R.C. Brammer, J.R. Helliwell, W. Lamb, A. Liljas, P.R. Moore, A.W. Thompson, and K. Worthington. Submitted to Nuclear Instr. and Meth.

[2] S. Svensson, and R. Nyholm, Uppsala University Institute of Physics Report UUIP-1139, July 1985. (A limited number of copies of this report are available at Daresbury from RCB)

[3] D.E. Aspnes and S.M. Kelso, Nucl. Instr. and Meth. 195, 175 (1982).

[4] D.J. Hubbard and E. Pantos, Nucl. Instr. and Meth. 208, 319 (1983).

[5] B. Lai and F. Cerrina, Nucl. Instr. and Meth. A246, 337 (1986).

[6] A.W. Thompson and J.R. Helliwell, Daresbury Lab. Technical Memo DL/SCI/TM51E, Dec. 1986.

[7] G.N. Greaves, R. Bennett, P.J. Duke, R. Holt and V.P. Suller, Nucl. Instr. and Meth. 208, 139 (1983).

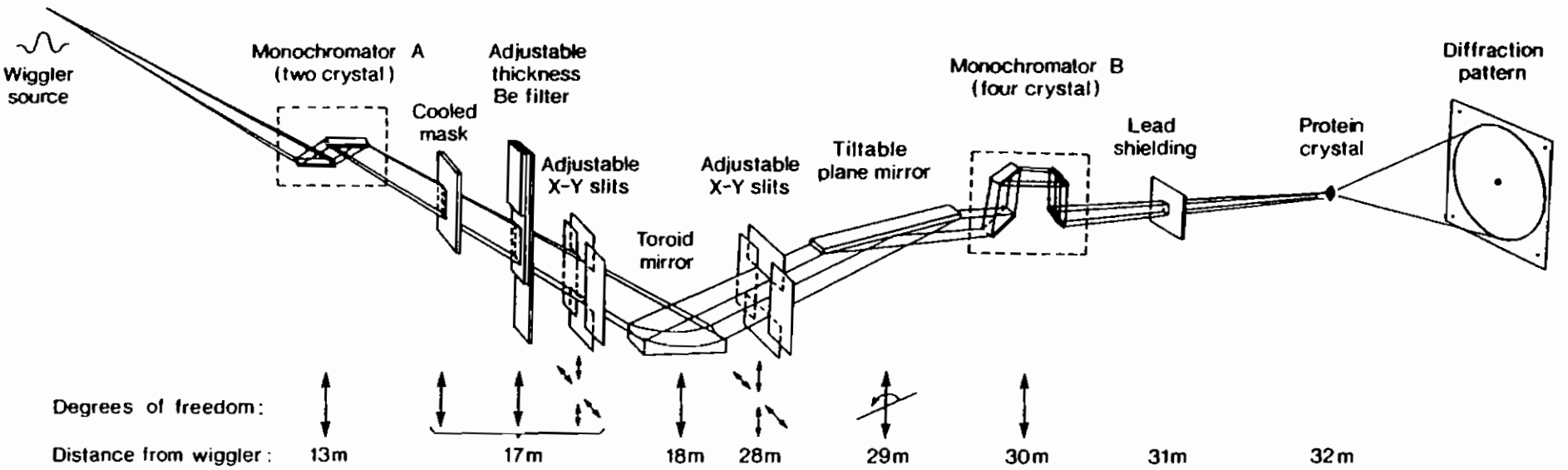
Wiggler source
Monochromator A (two crystal)
Cooled mask
Adjustable thickness Be filter
Adjustable X-Y slits
Toroid mirror
Adjustable X-Y slits
Tiltable plane mirror
Monochromator B (four crystal)
Lead shielding
Protein crystal
Diffraction pattern
Degrees of freedom:
Distance from wiggler:
13m
17m
18m
28m
29m
30m
31m
32m

Figure 1

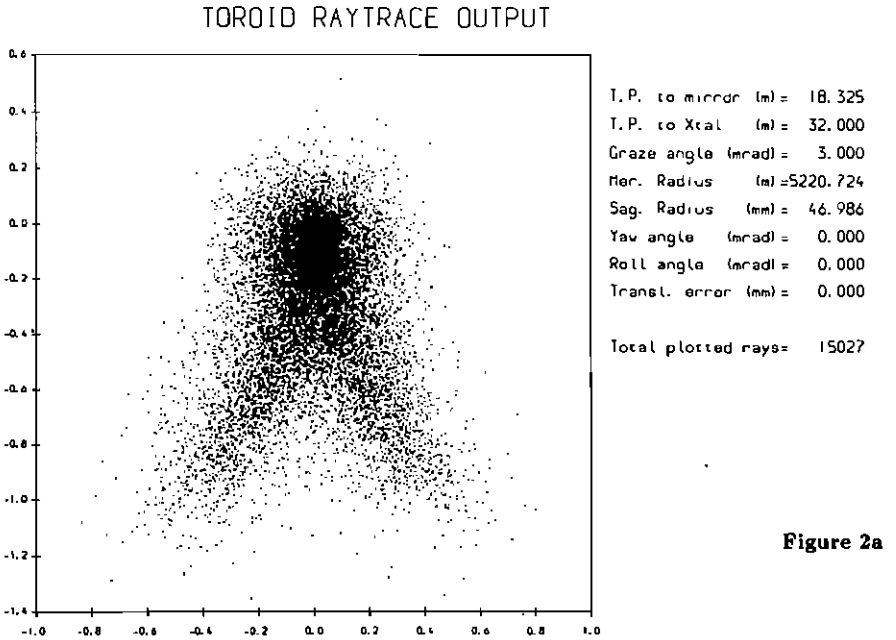

Figure 2a

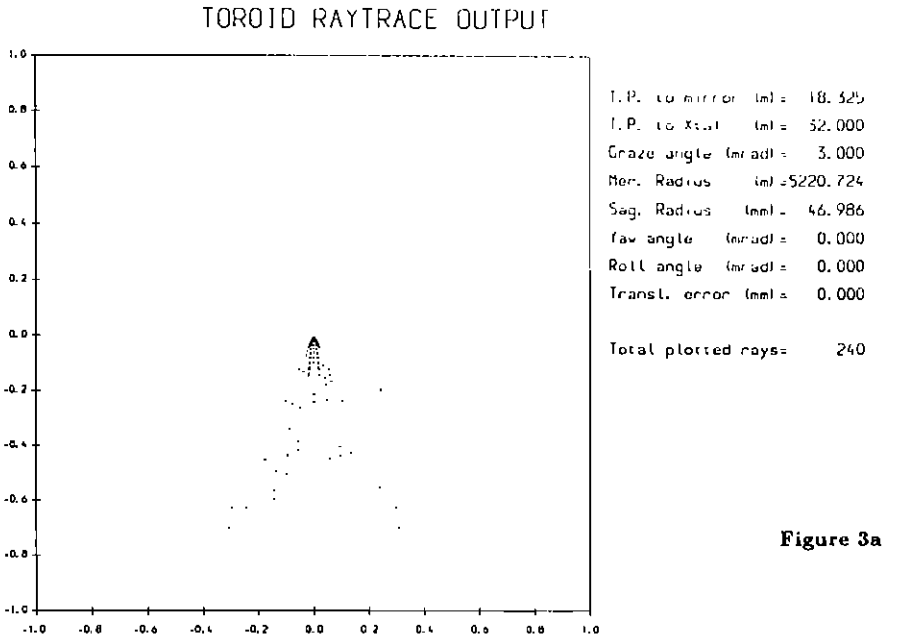

Figure 3a

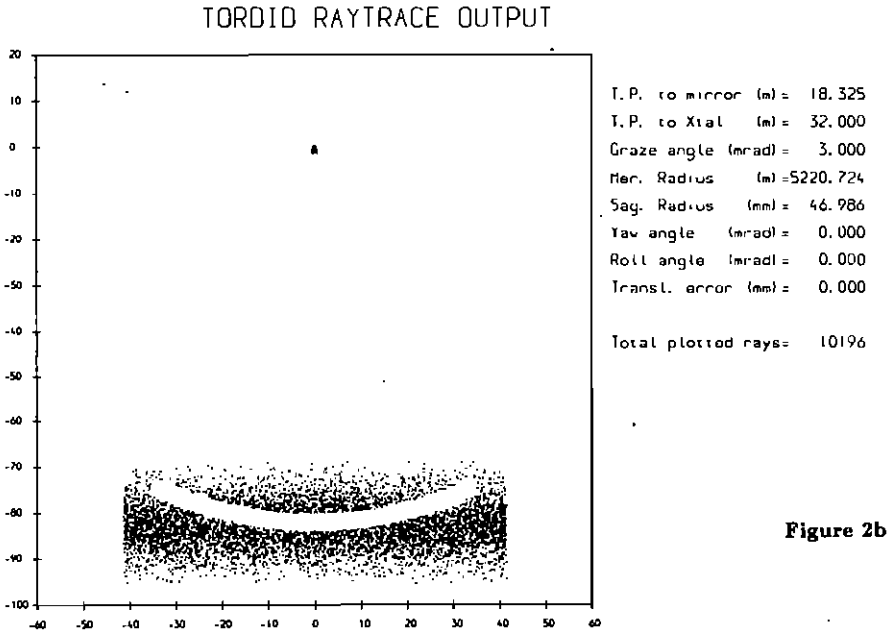

Figure 2b

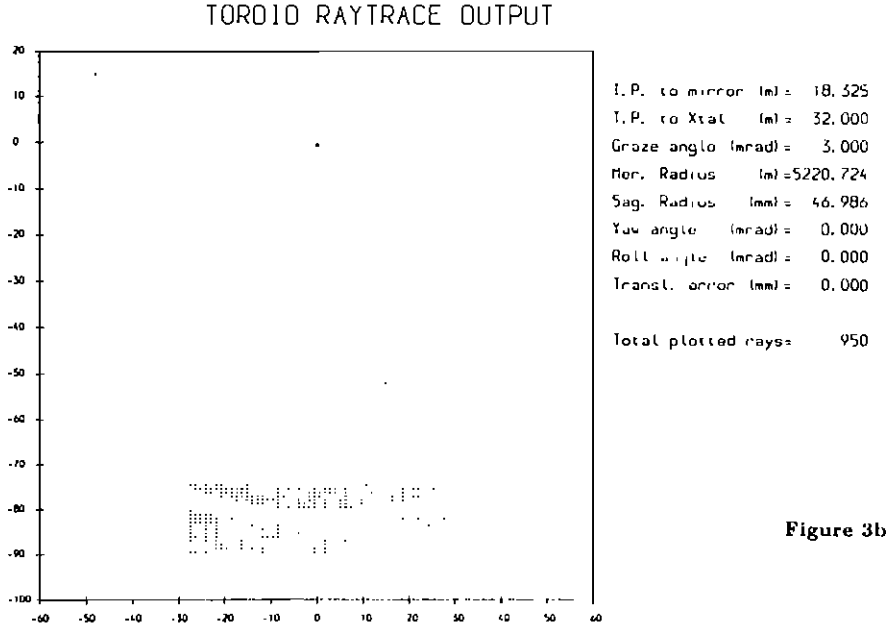

Figure 3b

PLANE MIRROR OUTPUT

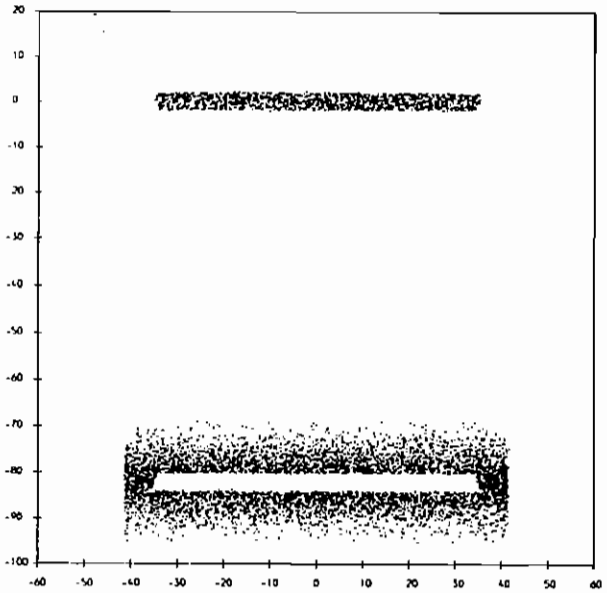

T.P. to mirror (m) = 18.325
T.P. to Xtal (m) = 32.000
Graze angle (mrad) = 3.000

Yaw angle (mrad) = 0.000
Roll angle (mrad) = 0.000
Transl. error (mm) = 0.000

Total plotted rays= 10196

Figure 4

CYLINDER RAYTRACE OUTPUT

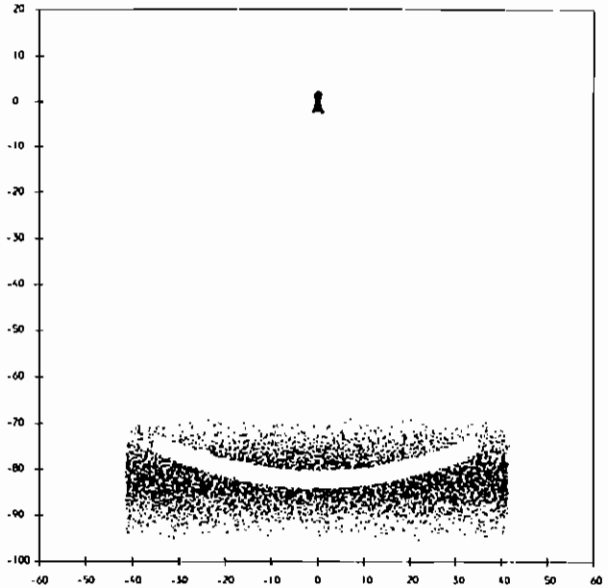

T.P. to mirror (m) = 18.325
T.P. to Xtal (m) = 32.000
Graze angle (mrad) = 3.000
Mer. Radius (m) = infinite
Sag. Radius (mm) = 46.986
Yaw angle (mrad) = 0.000
Roll angle (mrad) = 0.000
Transl. error (mm) = 0.000

Total plotted rays= 10196

Figure 5a

CYLINDER RAYTRACE OUTPUT

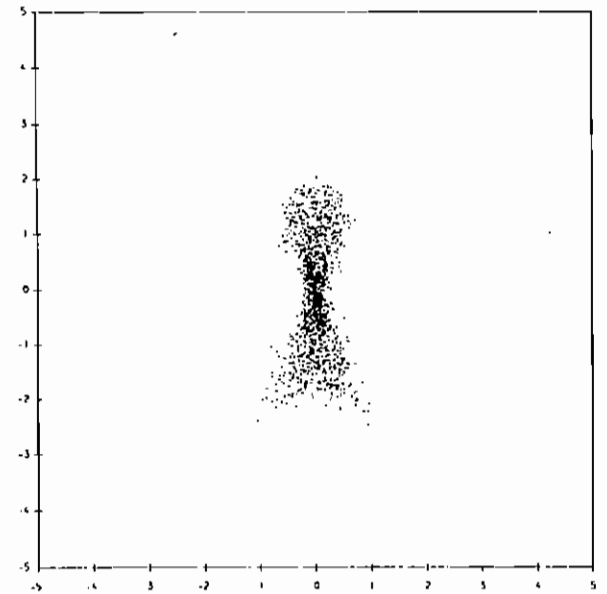

T.P. to mirror (m) = 18.325
T.P. to Xtal (m) = 32.000
Graze angle (mrad) = 3.000
Mer. Radius (m) = infinite
Sag. Radius (mm) = 46.986
Yaw angle (mrad) = 0.000
Roll angle (mrad) = 0.000
Transl. error (mm) = 0.000

Total plotted rays= 2251

Figure 5b

TOROID RAYTRACE OUTPUT

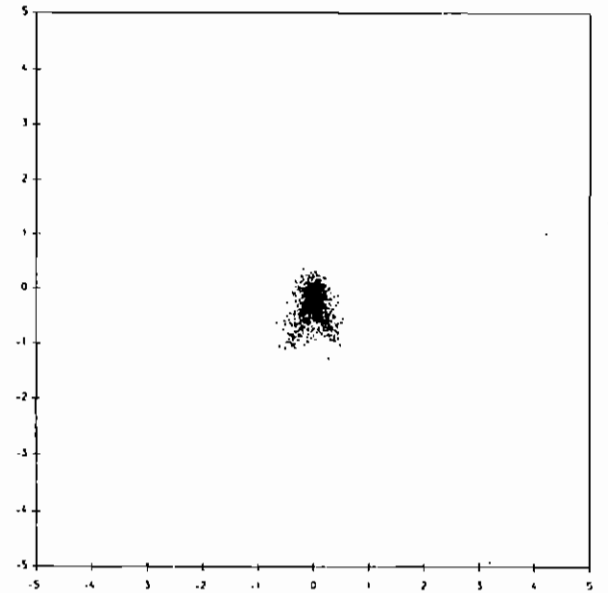

T.P. to mirror (m) = 18.325
T.P. to Xtal (m) = 32.000
Graze angle (mrad) = 3.000
Mer. Radius (m) = 5220.724
Sag. Radius (mm) = 46.986
Yaw angle (mrad) = 0.000
Roll angle (mrad) = 0.000
Transl. error (mm) = 0.000

Total plotted rays= 10196

Figure 6

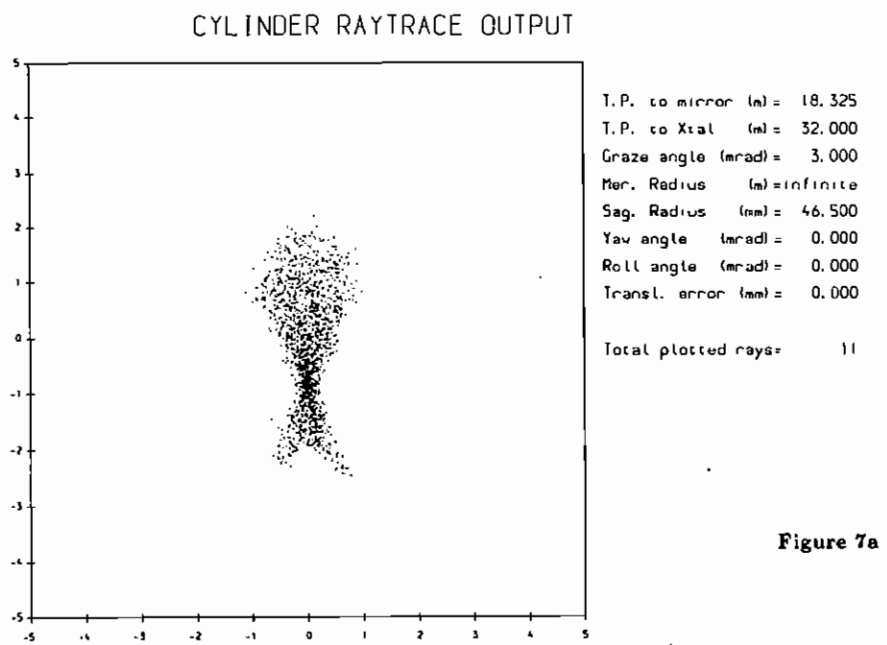

Figure 7a

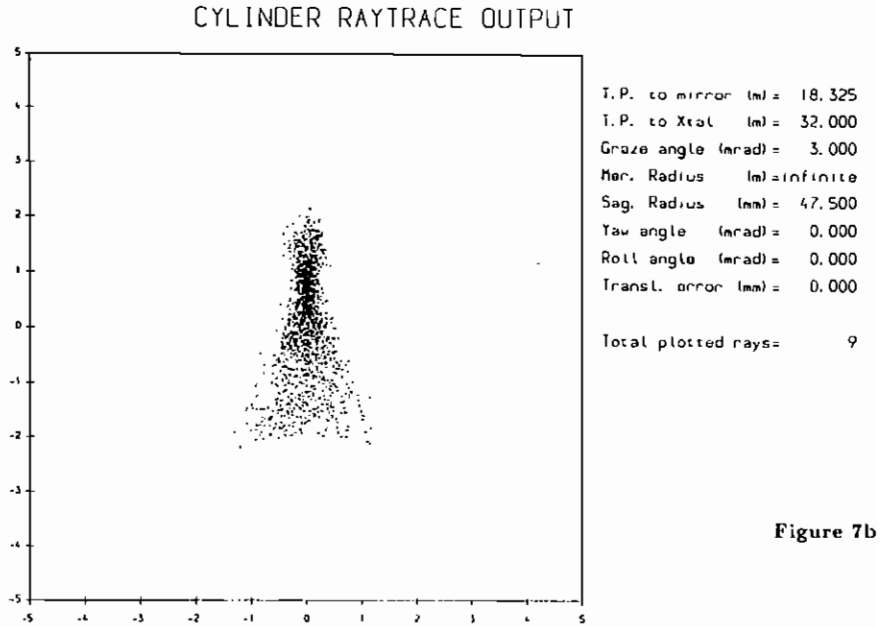

Figure 7b

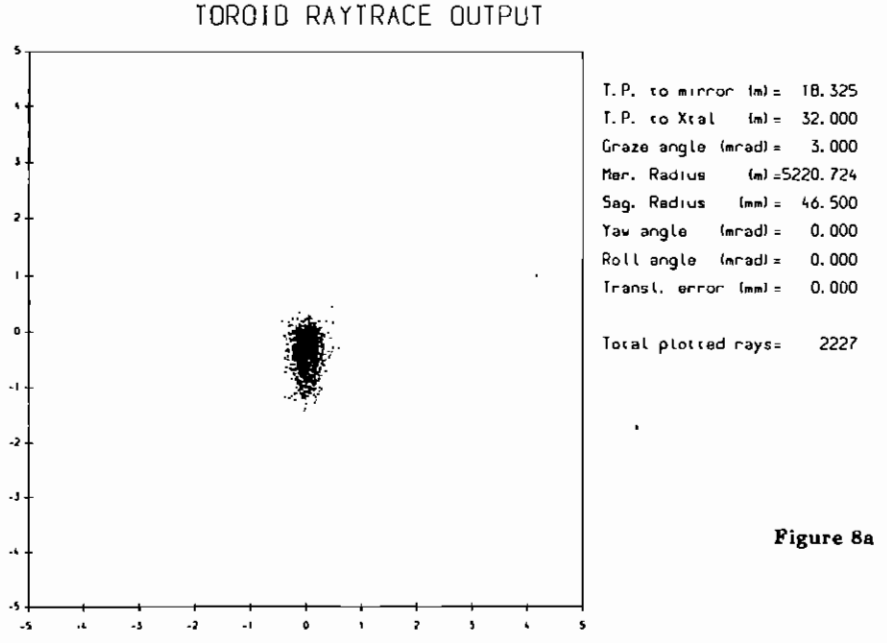

Figure 8a

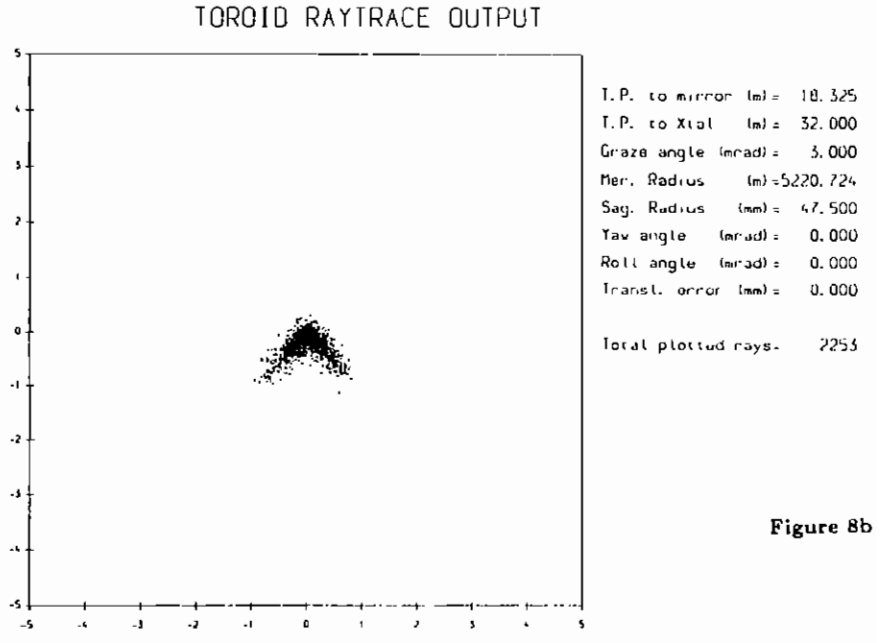

Figure 8b

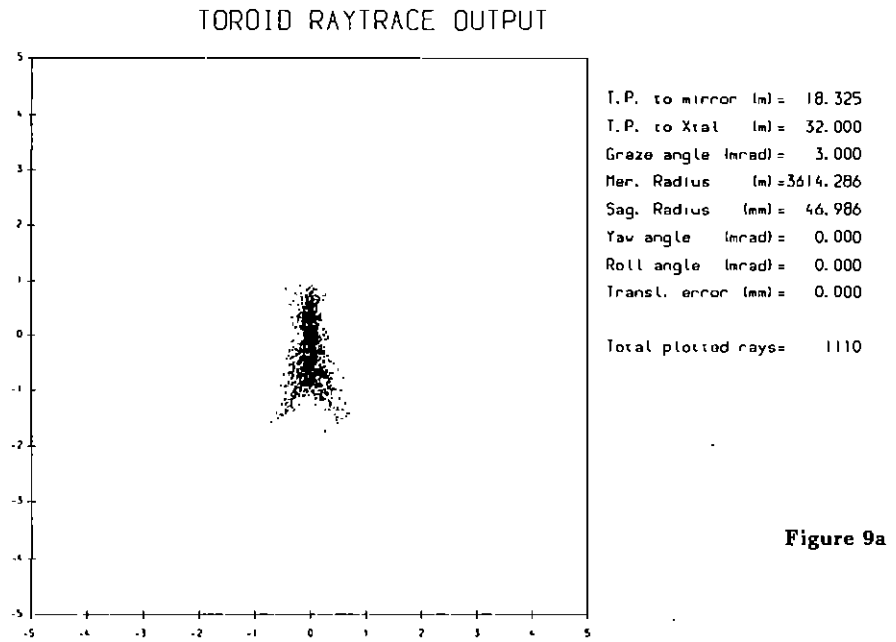

Figure 9a

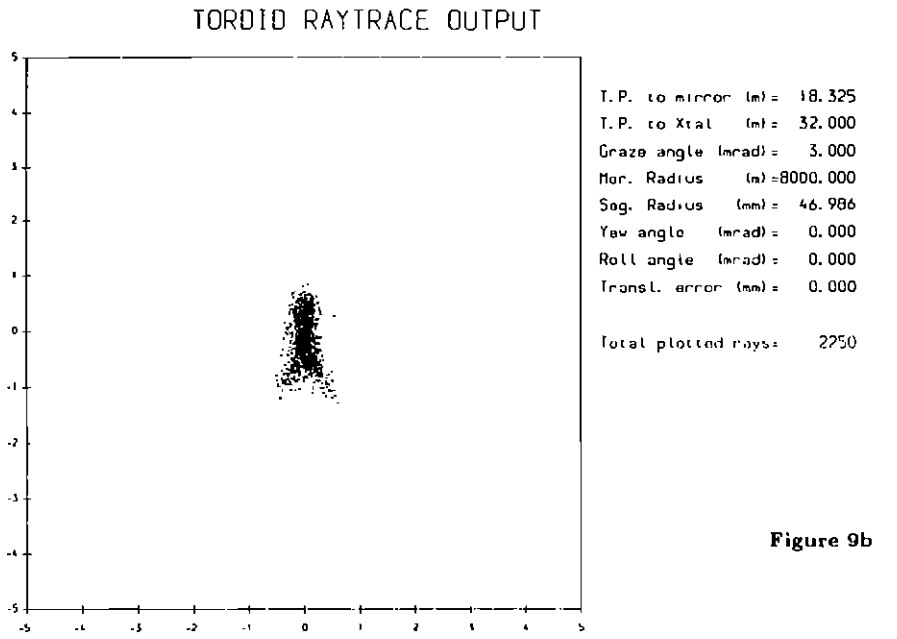

Figure 9b

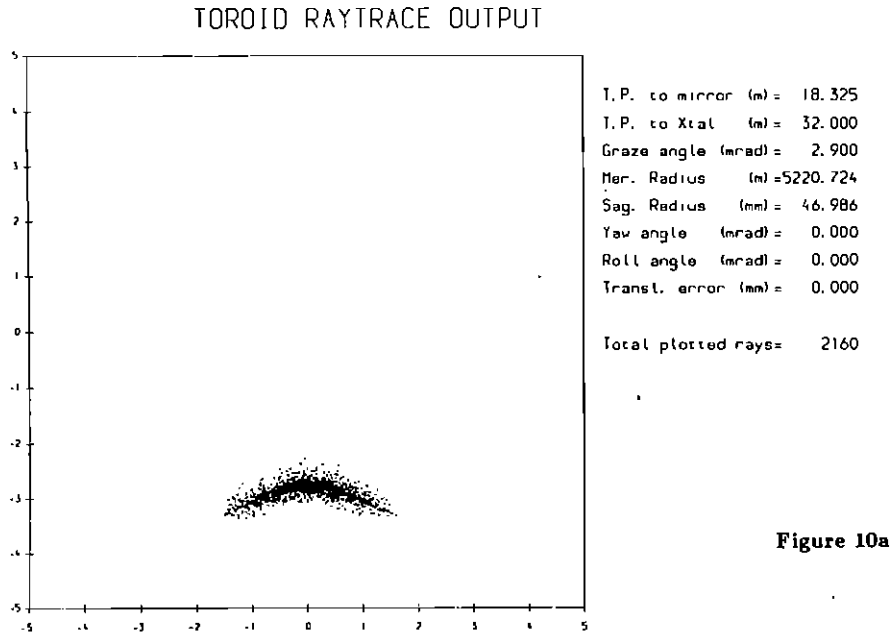

Figure 10a

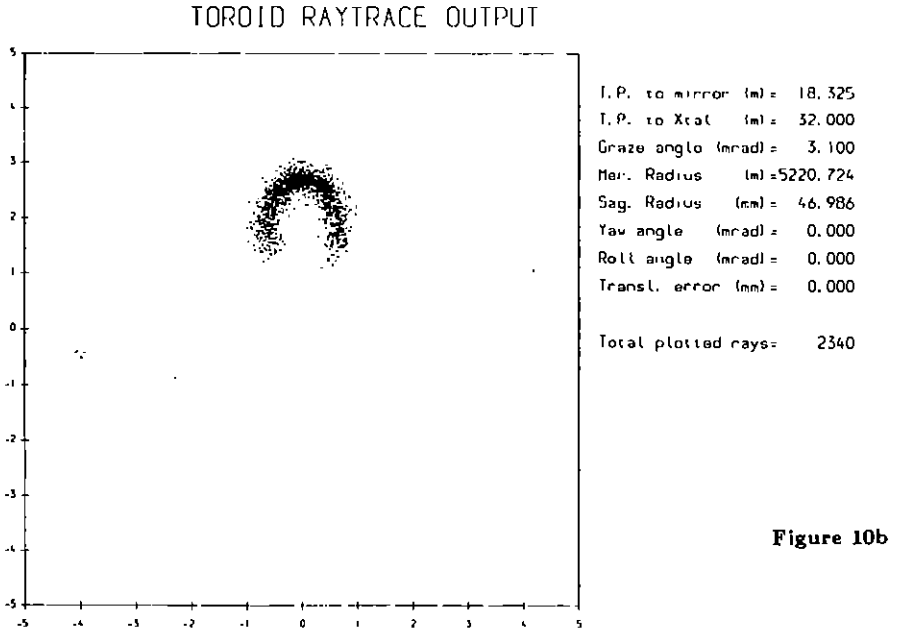

Figure 10b

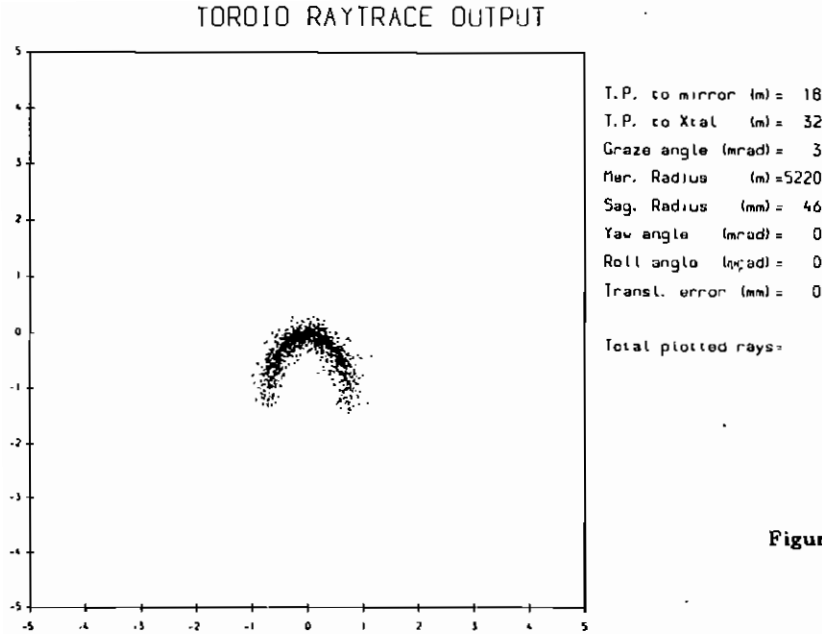

Figure 11a

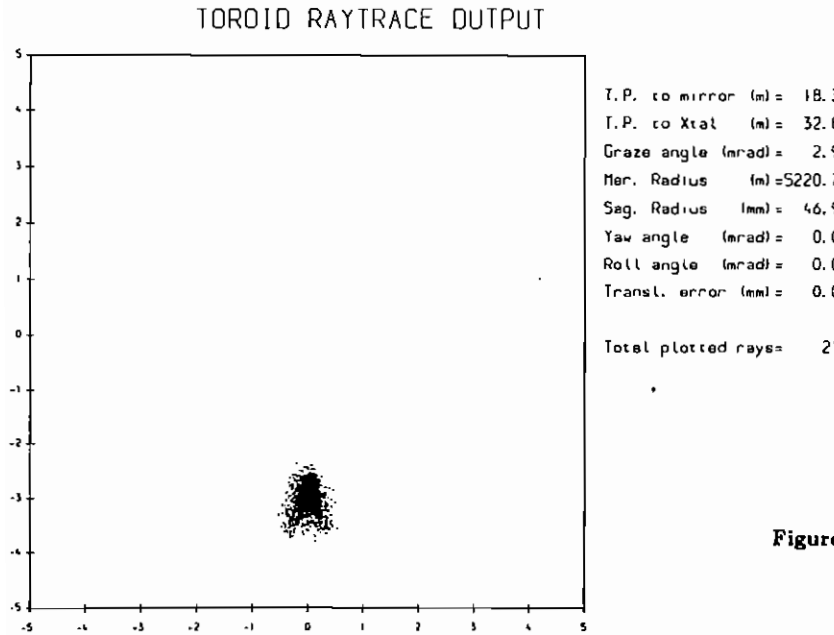

Figure 11b

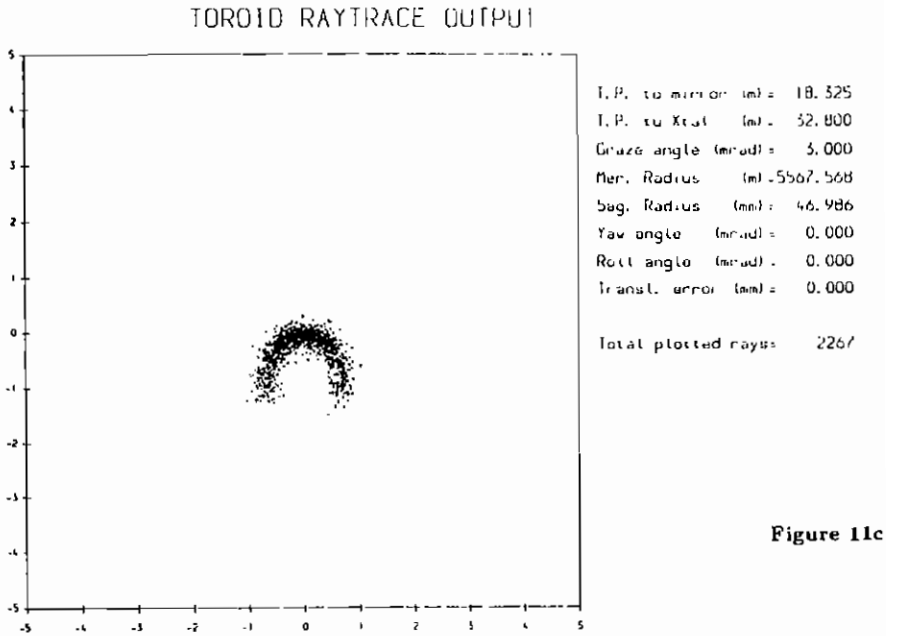

Figure 11c

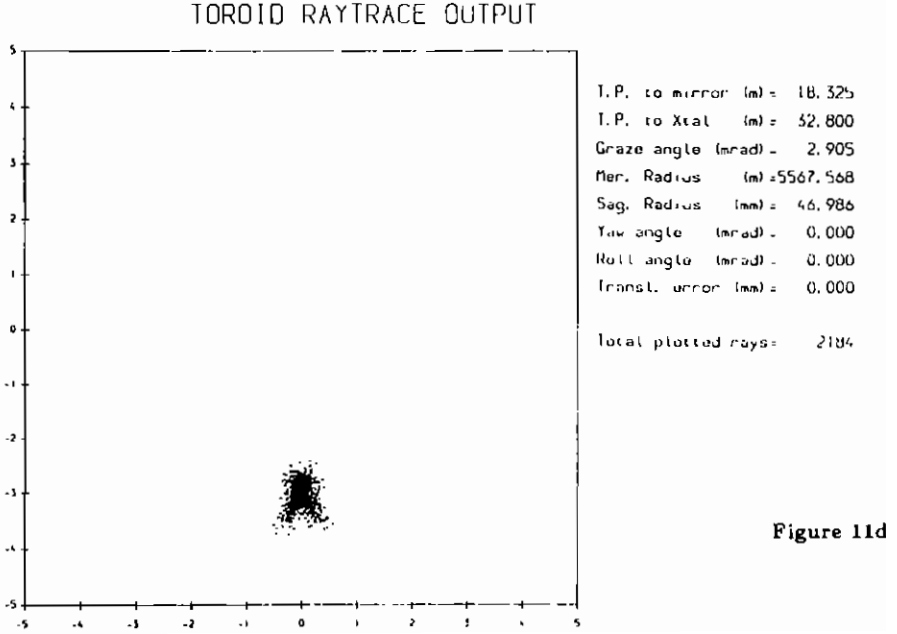

Figure 11d

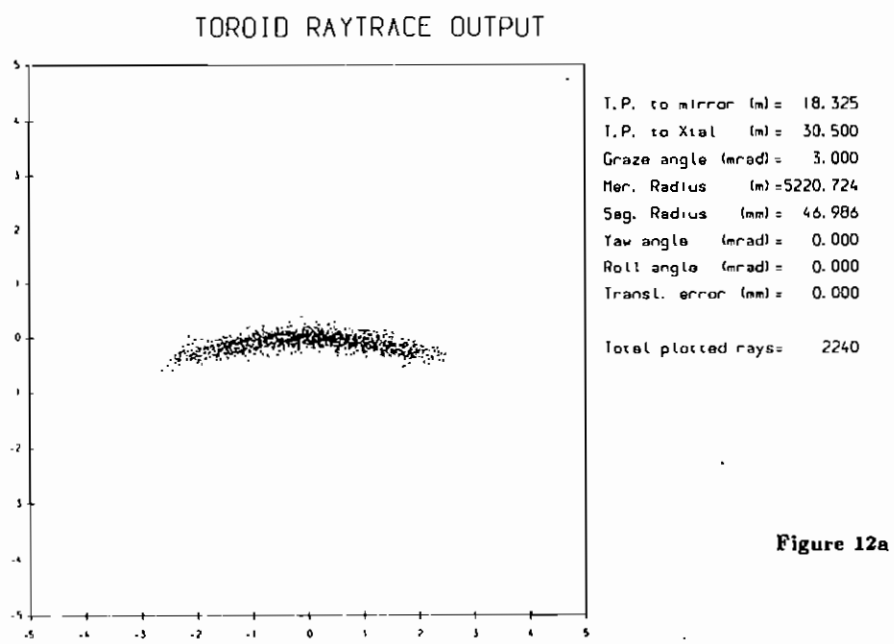

Figure 12a

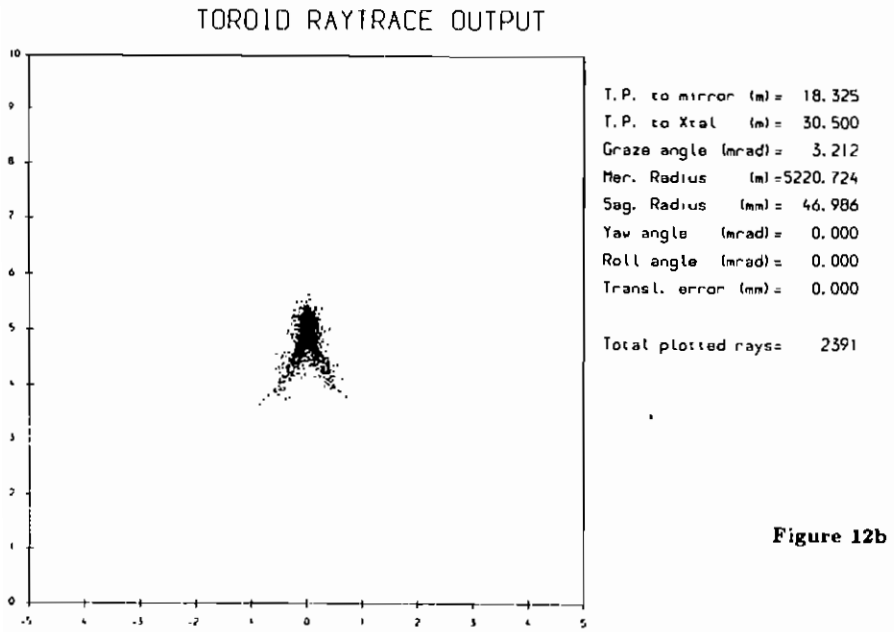

Figure 12b

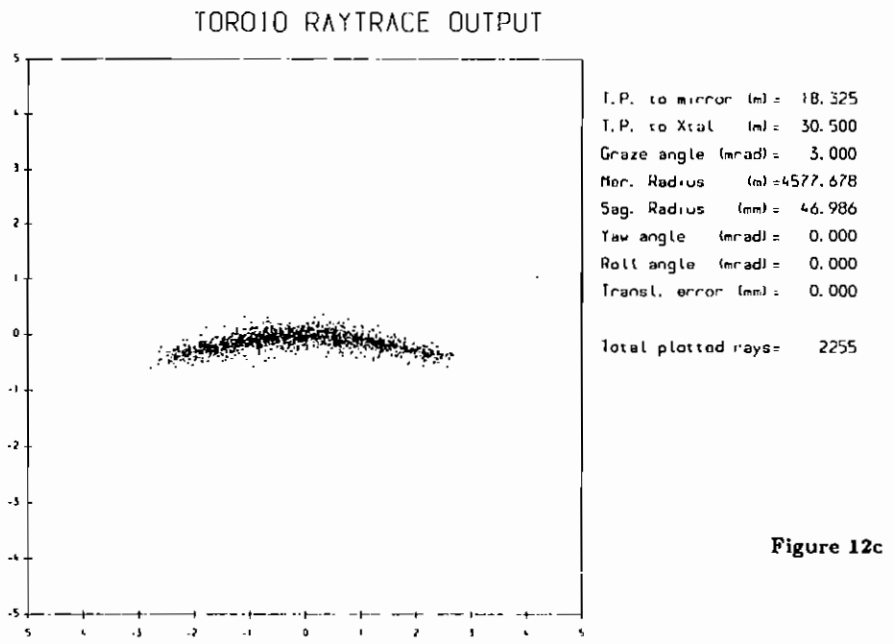

Figure 12c

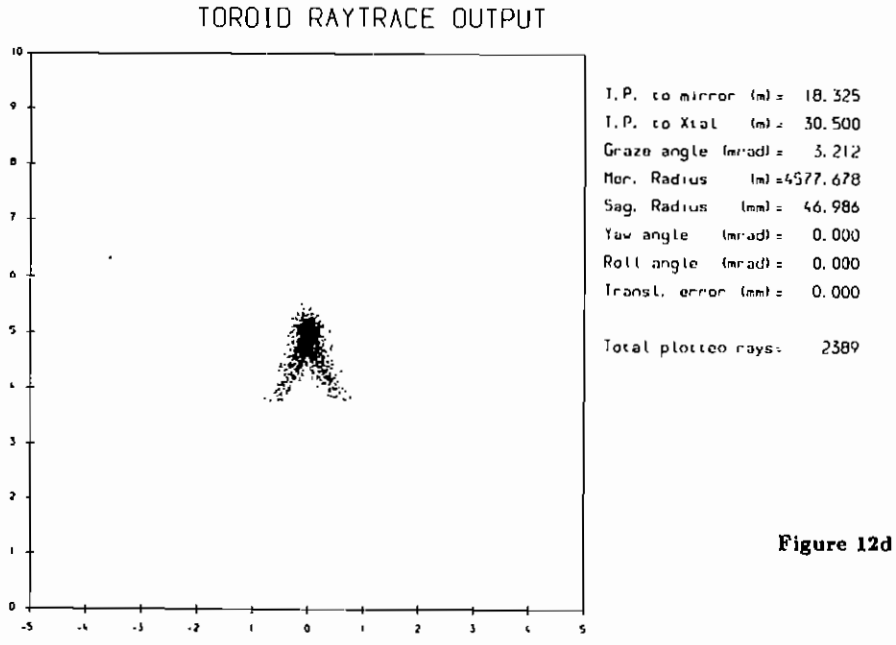

Figure 12d

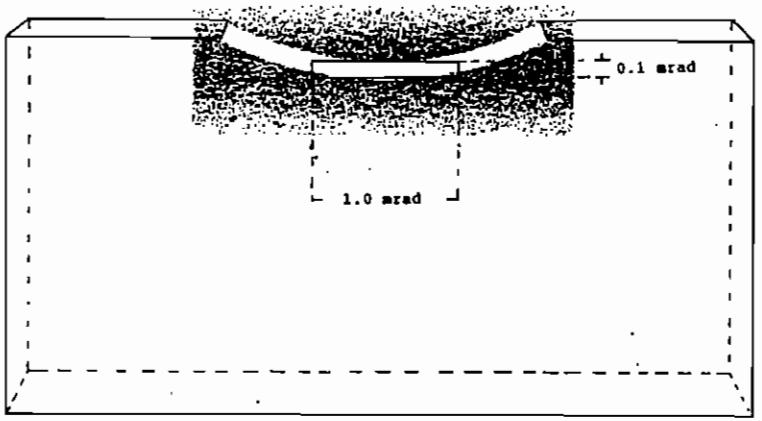

Figure 13

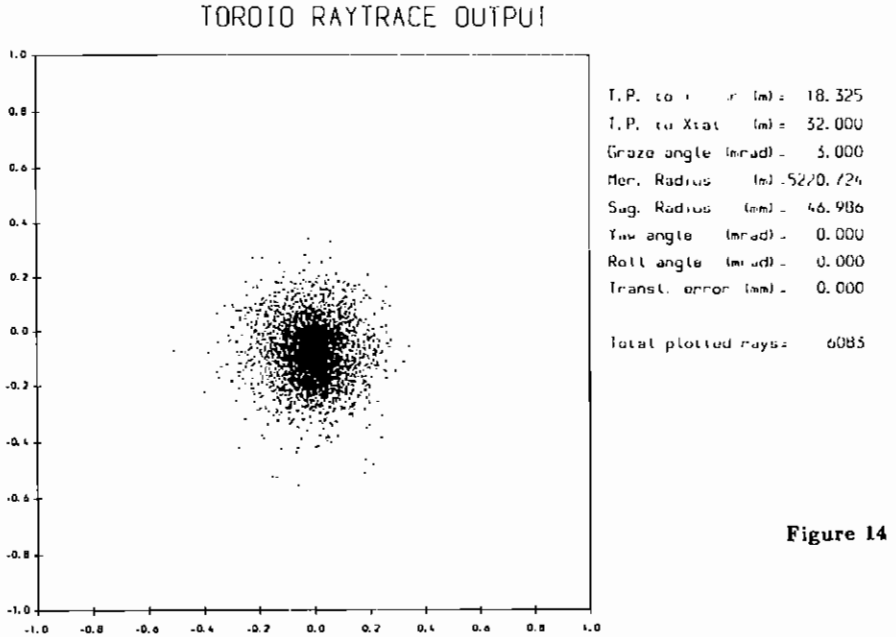

Figure 14

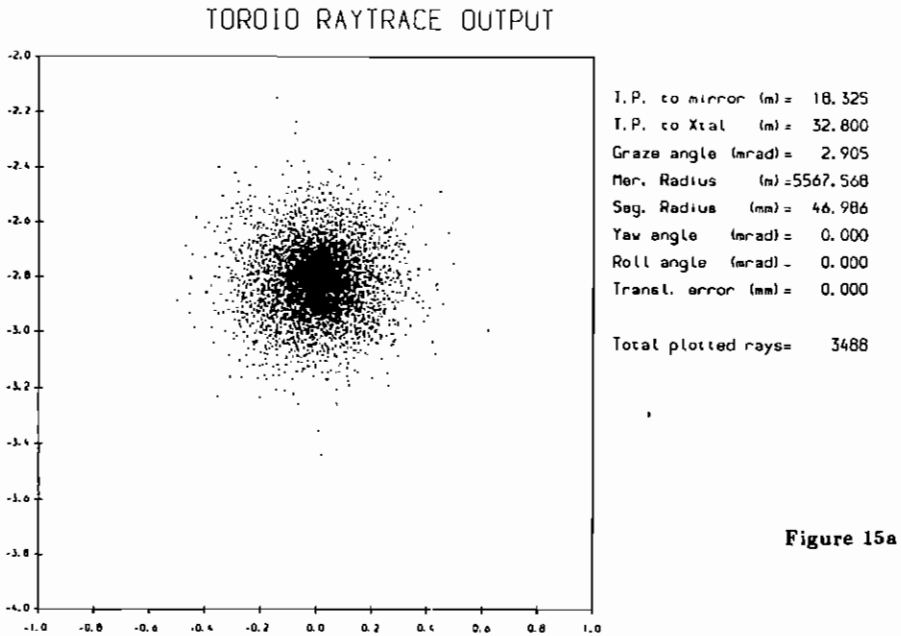

Figure 15a

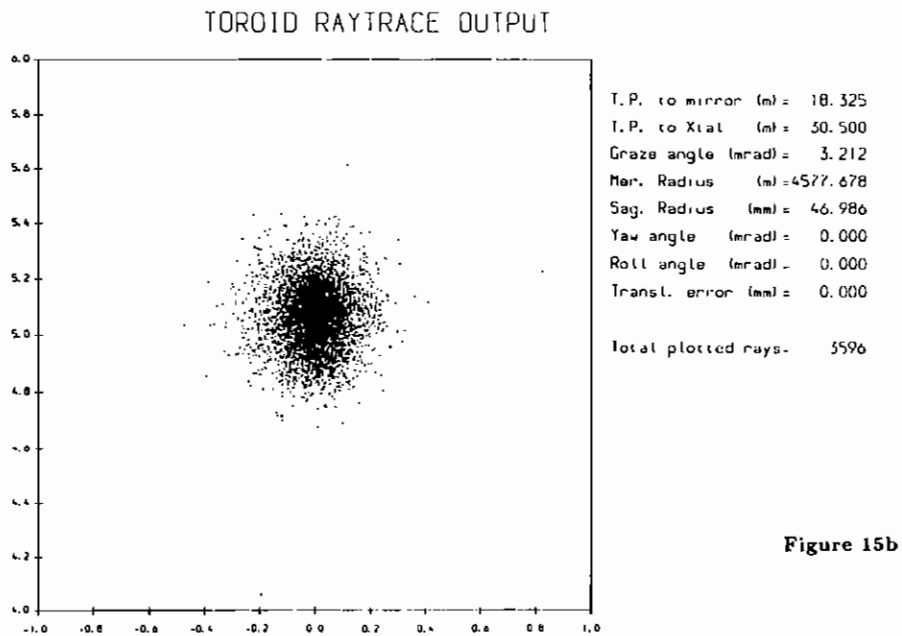

Figure 15b

TOROID RAYTRACE OUTPUT

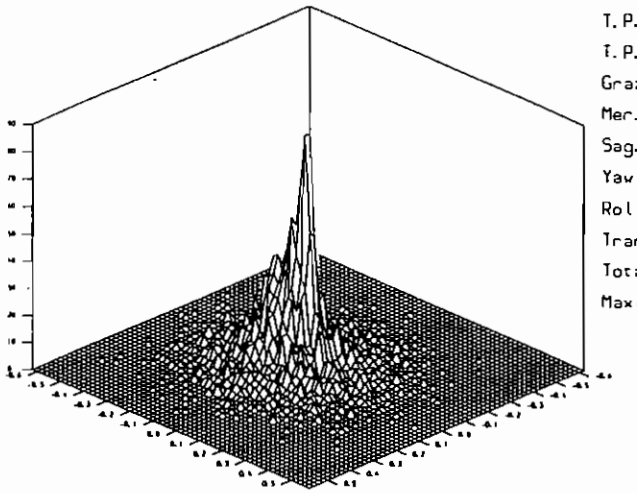

T. P. to mirror (m) = 18.325
T. P. to Xtal (m) = 32.000
Graze angle (mrad) = 3.000
Mer. Radius (m) = 5220.724
Sag. Radius (mm) = 46.986
Yaw angle (mrad) = 0.000
Roll angle (mrad) = 0.000
Transl. error (mm) = 0.000
Total plotted rays = 6085
Maximum z value = 87

Figure 16a

TOROID RAYTRACE OUTPUT

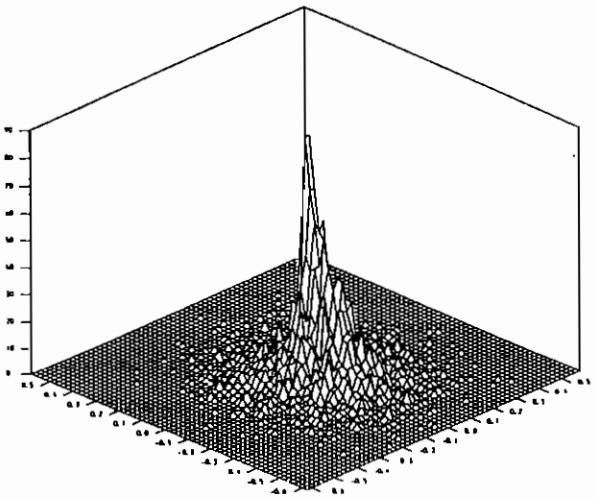

T. P. to mirror (m) = 18.325
T. P. to Xtal (m) = 32.000
Graze angle (mrad) = 3.000
Mer. Radius (m) = 5220.724
Sag. Radius (mm) = 46.986
Yaw angle (mrad) = 0.000
Roll angle (mrad) = 0.000
Transl. error (mm) = 0.000
Total plotted rays = 6085
Maximum z value = 87

Figure 16b

TOROID RAYTRACE OUTPUT

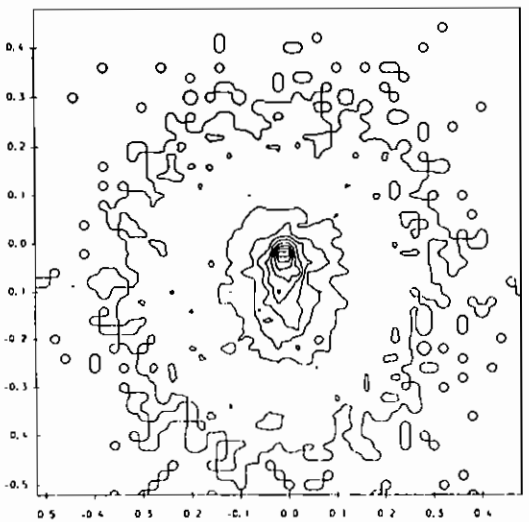

T. P. to mirror (m) = 18.325
T. P. to Xtal (m) = 32.000
Graze angle (mrad) = 3.000
Mer. Radius (m) = 5220.724
Sag. Radius (mm) = 46.986
Yaw angle (mrad) = 0.000
Roll angle (mrad) = 0.000
Transl. error (mm) = 0.000
Total plotted rays = 6085
Maximum z value = 87

Figure 17a

TOROID RAYTRACE OUTPUT

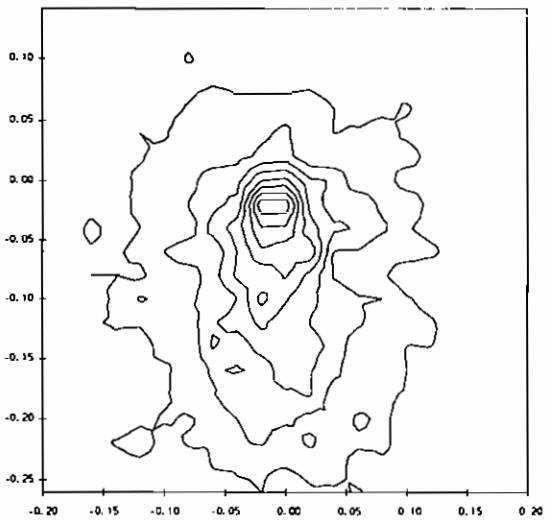

T. P. to mirror (m) = 18.325
T. P. to Xtal (m) = 32.000
Graze angle (mrad) = 3.000
Mer. Radius (m) = 5220.724
Sag. Radius (mm) = 46.986
Yaw angle (mrad) = 0.000
Roll angle (mrad) = 0.000
Transl. error (mm) = 0.000
Total plotted rays = 6085
Maximum z value = 87

Figure 17b

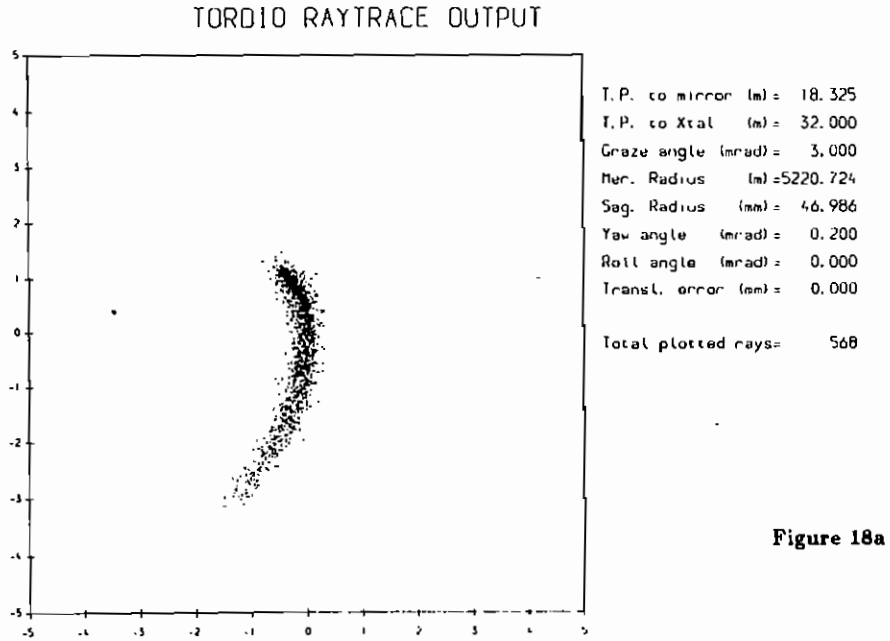

Figure 18a

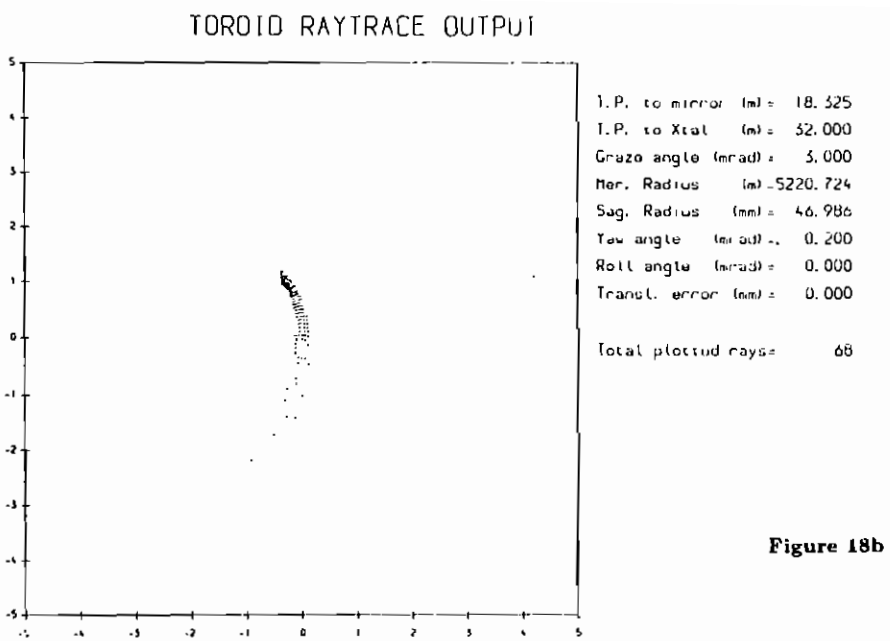

Figure 18b

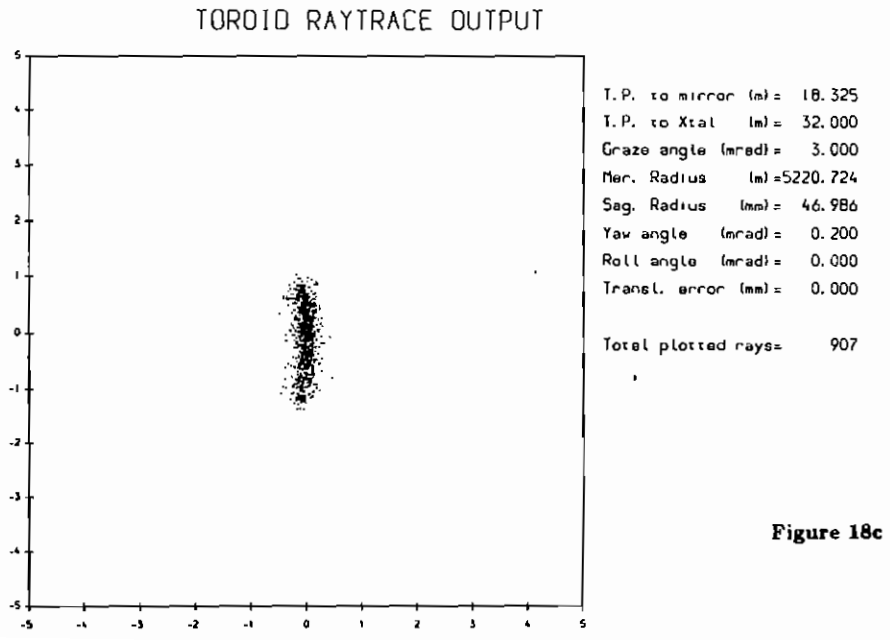

Figure 18c

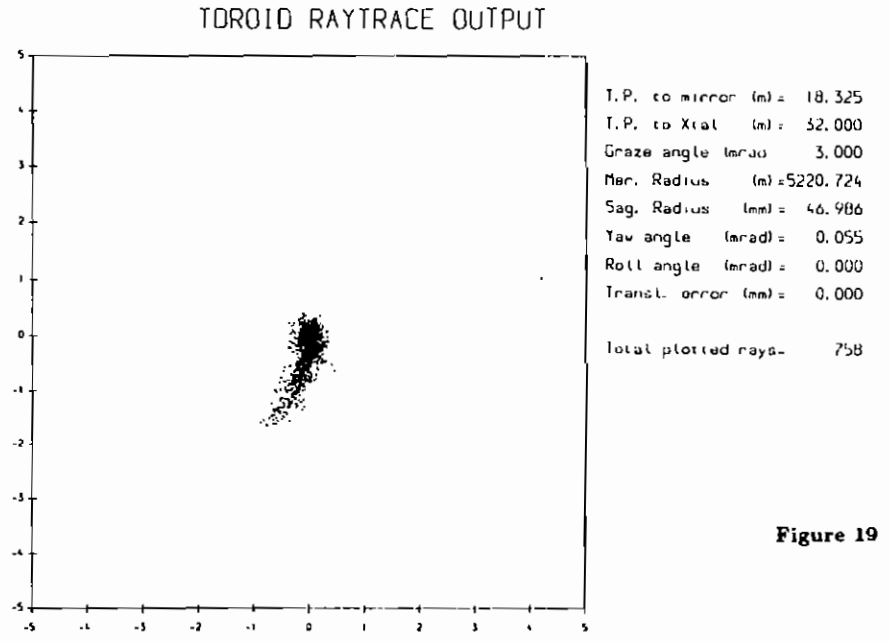

Figure 19

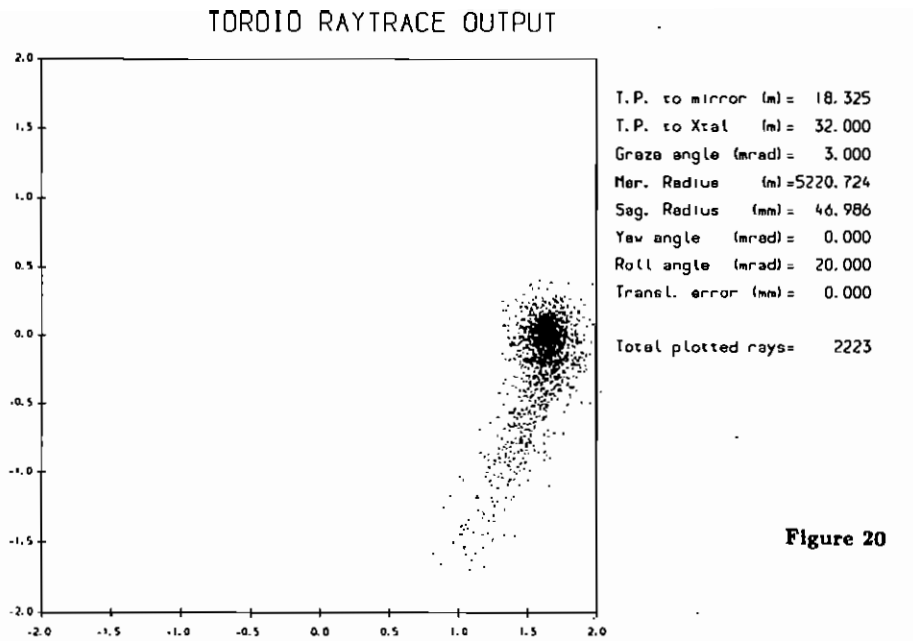

Figure 20

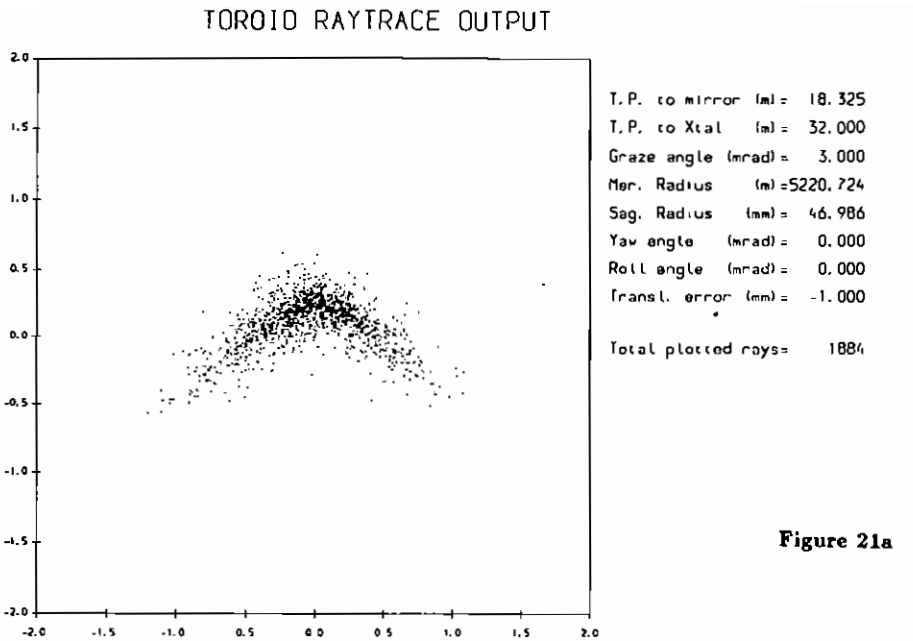

Figure 21a

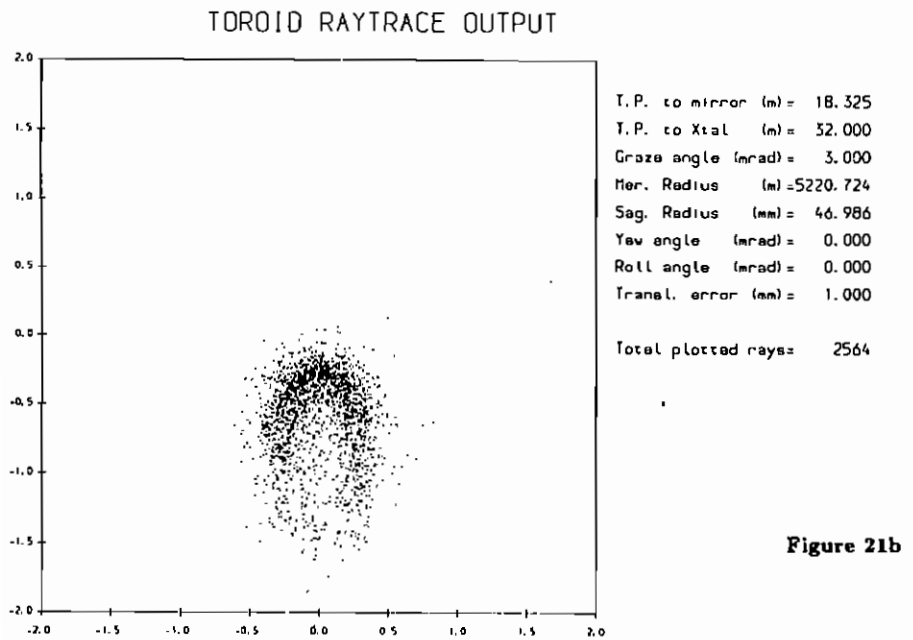

Figure 21b